

# Simplified Rotor and Stator Resistance Estimation Method Based on Direct Rotor Flux Identification

Mingyu Wang<sup>\*</sup>, Dafang Wang<sup>†</sup>, Guanglin Dong<sup>\*</sup>, Hui Wei<sup>\*</sup>, Xiu Liang<sup>\*</sup>, and Zexu Xu<sup>\*</sup>

<sup>†,\*</sup>Automotive Engineering College, Harbin Institute of Technology, Weihai, China

## Abstract

Since parameter mismatch seriously impacts the efficiency and stability of induction motor drives, it is important to accurately estimate the rotor and stator resistance. This paper introduces a method to directly calculate the rotor flux that is independent of stator and rotor resistance and electrical angle. It is based on obtaining the rotor and stator resistance using the model reference adaptive system (MRAS) method. The method has a lower computation burden and less adaptation time when compared with other rotor resistance estimation methods. This paper builds three coordinate frames to analyze the rotor flux error and rotor resistance error. A number of implementation issues are also considered.

**Key words:** MRAS, Induction motor, Reactive power, Rotor flux estimation, Rotor resistance, Stator resistance

## I. INTRODUCTION

Induction motor (IM) drives based on indirect field oriented control (IFOC) are popular in various industrial applications due to its dynamic performance and easy implementation. However, accurate flux orientation relies on knowledge of the motor parameters, especially the rotor resistance, which can drift with the operation temperature. There can be torque and flux errors, extra power losses, sluggish dynamics and so on [1]-[5], when a considerable error in the rotor resistance disrupts the precision field orientation, especially for medium-high volume motors with a small rotor resistance. Therefore, online rotor resistance identification is essential for IM drives.

There have been a lot of methods for online rotor resistance estimation, such as signal injection [6], [7], adaptive full-order observer (AFO) [8], [9], recursive least squares (RLS) [10], model reference adaptive system (MRAS) [11], [12] and so on. The main features of these methods are listed in Table I.

Among the methods listed above, MRAS is more attractive due to its simple structure and easy implementation [13]. MRAS consists of a reference model (independent of the variable), an adjustable model (correlated with the variable)

TABLE I  
FEATURES OF VARIOUS IDENTIFICATION METHODS

Type	QUALITY
Signal Injection	Adverse operation impact
Direct Calculation	More suitable offline
Full-order Observer	Vast matrix operation
RLS	Sensitive to noise
MRAS	Sensitive to parameters

and an adaptive mechanism. An adaptive mechanism, such as a PI controller, uses the error signal between two models to adjust the parameters. Depending on the chosen functional candidates, such as the rotor flux, stator voltage [14], electromagnetic torque [15] and reactive power [16], various MRAS-based rotor resistance estimation techniques have been proposed. A unified model was developed in [17], which shows that types of MRAS-based models are united in essence and share a unified mathematical expression. To avoid flux estimation, a rotor resistance adaptation real-time method utilizing reactive power was proposed in [13]. The sensitivity and stability are analyzed in detail with the Popov hyperstability concept. Although the system can converge to a real value, it adjusts the rotor resistance and rotor speed in real time, which can cause vibrations under the instantaneous load-change condition. In [15], a particular relationship between the sign of the reactive power error and the sign of the rotor resistance error was pointed out. In [18], a compensation for dead time and time delays was considered

Manuscript received Jun. 13, 2018; accepted Jan. 9, 2019

Recommended for publication by Associate Editor Gaolin Wang.

<sup>†</sup>Corresponding Author: wdfcjl@163.com

Tel: +86-138-6300-9863, Fax: 0631-5687212, China

<sup>\*</sup>Automotive Engineering College, Harbin Institute of Tech., China

to reduce identification errors.

In this paper, the influence of errors in rotor resistance is investigated in detail. Depending on the application of equations in different frames, the real rotor flux of an IM, which does not suffer from integrator-related problems [19], [20], is directly calculated. The uniqueness of this method is that the rotor flux can be acquired directly and that it is independent of stator and rotor resistance and electrical angle. Then the rotor flux is used to adjust the rotor resistance and stator resistance. In order to eliminate reactive power errors, the voltage distortion caused by dead time and time delay is compensated. The scheme is simulated in Simulink and a prototype is developed to validate the technique. Extensive simulation and experimental results are presented to demonstrate the performance of the algorithm.

II. INFLUENCE OF ROTOR RESISTANCE ERROR

A. Vector Control System for Induction Motors

The dynamic model of an IM in the synchronous reference frame is given by (1), with the stator current and rotor flux selected as state variables.

$$P \begin{bmatrix} I_s \\ \psi_r \end{bmatrix} = \begin{bmatrix} A_{11} & A_{12} \\ A_{21} & A_{22} \end{bmatrix} \begin{bmatrix} I_s \\ \psi_r \end{bmatrix} + \frac{1}{\sigma L_s} U_s \quad (1)$$

Where:

$$\begin{aligned} A_{11} &= -\left[ \frac{R_s}{\sigma L_s} + \frac{(1-\sigma)R_r}{\sigma L_r} \right] I, A_{12} = -\frac{L_m}{\sigma L_s L_r} (-\frac{R_r}{L_r} I + \omega_{re} J) \\ A_{21} &= \frac{L_m R_r}{L_r} I, A_{22} = -\frac{R_r}{L_r} I + \omega_{re} J \\ I &= \begin{bmatrix} 1 & 0 \\ 0 & 1 \end{bmatrix}, J = \begin{bmatrix} 0 & -1 \\ 1 & 0 \end{bmatrix}, \sigma = 1 - \frac{L_m^2}{L_s L_r} \end{aligned}$$

The symbol ‘P’ is the differential operator.

The symbol ‘ $\omega_{re}$ ’ is the electrical angular velocity of the motor.

The symbols ‘ $L_s$ ,  $L_r$  and  $L_m$ ’ are stator inductance, rotor inductance and mutual inductance, respectively.

The rotor flux can be expressed as:

$$\psi_r = L_m I_M \quad (2)$$

The electromagnetic torque equation is as follows:

$$T_e = \frac{3}{2} p \frac{L_m}{L_r} \psi_{rM} I_T \quad (3)$$

The symbol ‘p’ refers to the pole pairs of the motor.

The slip frequency ‘ $\omega_f$ ’ can be calculated as:

$$\omega_f = \frac{R_r}{L_r} \cdot \frac{I_T}{I_M} \quad (4)$$

In the case of the vector control system, the slip frequency relationship in (4) is used for calculating the rotor flux vector position as follows:

$$\theta_e = \int (\omega_{re} + \omega_f) dt \quad (5)$$

Fig. 1 shows a typical scheme of an IM indirect vector control system. For a properly designed current loop in the MT

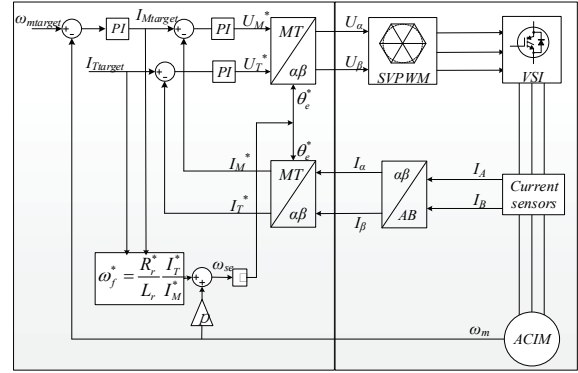


Fig. 1. Scheme of an IM vector control system.

reference frame, the stator currents  $I_M^*$  and  $I_T^*$  are assumed to keep tracking their target values  $I_{Mtarget}$  and  $I_{Ttarget}$  tightly. Therefore, in the following analysis, the measured current values are considered to be equal to their target value in the steady state.  $X^*$  represents variables obtained when the used rotor resistance is a wrong value  $R_r^*$ . In particular,  $X^* = X$  such as  $I_M^* = I_M$  when  $R_r^* = R_r$ . This means that the IM runs in the ideal situation.

B. Influence of Rotor Resistance Errors in Three Frames

The influence of rotor resistance errors will be analyzed in three coordinate frames. Suppose  $R_r$  is the actual rotor resistance and  $R_r^*$  is the rotor resistance used in the control system. The first frame can be called the control frame, marked as  $M^* - T^*$ . In this frame, the rotor flux is oriented in the wrong rotor resistance  $R^*$ . The second frame can be called the real frame, marked as  $M^c - T^c$ . In this frame, the rotor resistance is still oriented in the wrong value. The first and second frames are both built in the real control system. The third frame is regarded as an ideal frame, marked as  $M - T$ . This frame only exists when the control frame aligns with the real frame or  $R_r^* = R_r$ .

Since  $U_\alpha, U_\beta$  and  $I_\alpha, I_\beta$  are real values for an actual IM and  $I_\alpha, I_\beta$  are the functional results of  $U_\alpha, U_\beta$  in the real rotor resistance R in a control system, the second frame sets up a bridge between the first and the third frame, which needs to be discussed here. Fig. 2 shows the relationship between the first and second frames.

Rotor flux orientation uses  $\omega_{se}^*$  as the electrical speed. Thus,  $U_\alpha, U_\beta$  are achieved in  $\omega_{se}^*$ , which satisfies:

$$\omega_{se}^c = \omega_{se}^* \quad (6)$$

In particular, when rotor speed is acquired accurately, the electrical speed satisfies:

$$\begin{cases} \omega_{se}^c = \omega_{se}^* > \omega_{se} & R_r^* > R_r \\ \omega_{se}^c = \omega_{se}^* < \omega_{se} & R_r^* > R_r \\ \omega_{se}^c = \omega_{se}^* = \omega_{se} & R_r^* > R_r \end{cases} \quad (7)$$

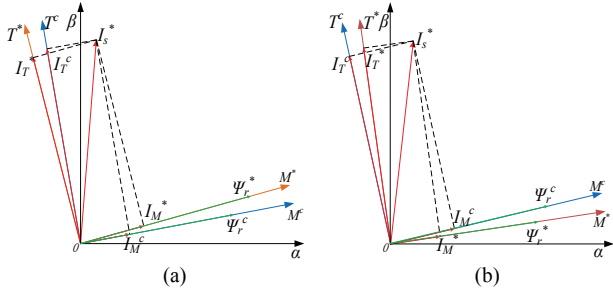


Fig. 2. Variable comparisons in the first and second frame. (a)  $R_r^* > R_r$ . (b)  $R_r^* < R_r$ .

$I_s^*$  in Fig. 2, which represents the stator current vector, is projected into the  $M^*-T^*$  and  $M^c-T^c$  frames.  $I_M^c$  is the field current in the second frame and real rotor flux can be obtained.

$$\psi_r^c = L_m I_M^c \quad (8)$$

$I_M^*$  is the field current in the first frame, which is assumed to track the reference value  $I_{M\text{target}}$  in the control system. The rotor flux calculated in the first frame and real rotor flux in the second frame satisfy the following:

$$\psi_r^* = L_m I_M^* = L_m I_M^c \sqrt{\frac{I_M^{c2} + I_T^{c2}}{I_M^2 + \left(\frac{R_r}{R_r^*}\right)^2 I_T^2}} = \psi_r^c \sqrt{\frac{I_M^2 + I_T^2}{I_M^2 + \left(\frac{R_r}{R_r^*}\right)^2 I_T^2}} \quad (9)$$

Resolving  $\psi_r^*$  to the  $M^c-T^c$  frame yields:

$$\begin{cases} \psi_{rM}^* = \psi_{rM}^c \frac{I_M^2 + \frac{R_r}{R_r^*} I_T^2}{\left(\frac{R_r}{R_r^*}\right)^2 I_T^2 + I_M^2} \\ \psi_{rT}^* = \psi_{rT}^c \frac{I_M I_T - \frac{R_r}{R_r^*} I_M^c I_T^c}{\left(\frac{R_r}{R_r^*}\right)^2 I_T^2 + I_M^2} \end{cases} \quad (10)$$

The third frame is obtained when the first frame aligns with the second frame or  $R_r^* = R_r$ , and (10) takes a simplified form as:

$$\begin{cases} \psi_{rM}^* = \psi_{rM}^c = \psi_{rM} = L_m I_M \\ \psi_{rT}^* = \psi_{rT}^c = \psi_{rT} = 0 \end{cases} \quad (11)$$

In the case of  $R_r^* \neq R_r$ , subtracting (10) from (11), shows that the signs of the rotor flux errors are directly correlated with detuning of the rotor resistance as:

$$\begin{cases} (\psi_{rM}^c - \psi_{rM}^*) (R_r - R_r^*) \geq 0 \\ I_T^c (0 - \psi_{rT}^*) (R_r - R_r^*) \geq 0 \end{cases} \quad (12)$$

The inequalities of (12) can explain that the field current and torque current in the second frame are larger than those in the first frame when rotor resistance satisfies  $R_r^* < R_r$ . In

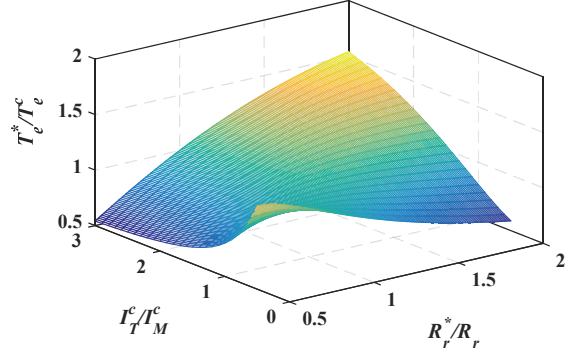


Fig. 3. Error in electromagnetic torque.

TABLE II  
ACIM PARAMETERS

Variables	QUANTITY	Unit
Rated Power	150	W
Rated Voltage	220	V
Rated Current	6	A
Rated Frequency	60	Hz
Rated Speed	1726	rpm
Stator Resistor/Inductance	11.0/0.316	$\Omega/H$
Rotor Resistor/Inductance	6.1/0.316	$\Omega/H$
Mutual Inductance	0.294	H

addition, it is the same in reverse.

Due to the error in the rotor flux, there must be some errors in the magnetic torque of the IM. Considering (3) and (10), the torque calculated in the first frame and the real torque in the second frame satisfy:

$$T_e^* = T_e^c \cdot \frac{I_M^2 + I_T^2}{\frac{R_r^*}{R_r} I_M^2 + \frac{R_r}{R_r^*} I_T^2} \quad (13)$$

Equation (13) shows that the torque error  $T_e^*/T_e^c$  is correlated with  $R_r^*/R_r$  and  $I_T^c/I_M^c$ . Fig. 3 shows the relationships among the three variables.

### C. Simulation of the Rotor Resistance Error Influence

Since all of the values in the first and second frame can be obtained in simulation, the validation is carried out in simulation. The parameters in the simulation, like those in the experiment, are shown in Table II.

When the motor speed is kept at 100r/min, the updating process when  $I_M^* = 1A$  is presented in Fig. 4 and Fig. 5. The load torque is set at 0.4N·m, 0.7N·m and 1N·m at the times 0.4s, 1.2s and 1.7s, respectively. The difference between Fig. 4 and Fig. 5 is that Fig.4 simulates at  $R_r^* = 0.5R_r$  while Fig. 5 simulates at  $R_r^* = 2R_r$ .

To verify the theory, one point was chosen to test.  $I_M^c = 0.53$ ,  $I_T^c = 2.37$ ,  $\psi_r^c = 0.16$ ,  $\psi_r^* = 0.29$ ,  $T_e^c = 1.03$  and  $T_e^* = 1.81$  can be obtained in the steady state when  $R_r^* = 2R_r$  and  $T_e^c = 1$  in Fig. 5. The results calculated by the feedback

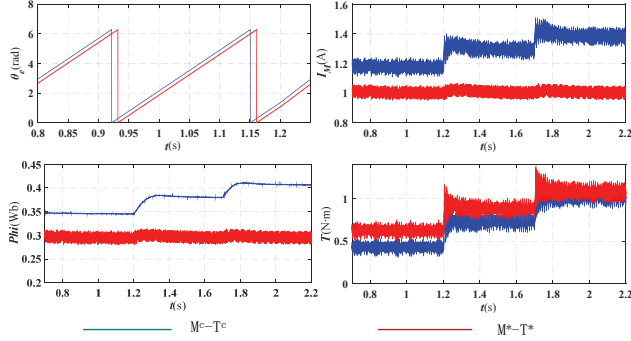


Fig. 4. Comparison of the electrical angle, field current, rotor flux and torque when  $R_r^* = 0.5R_r$ .

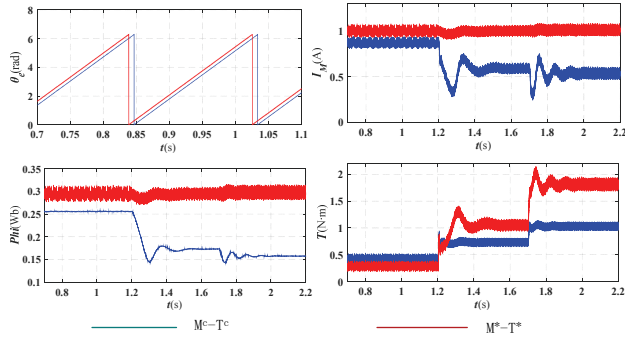


Fig. 5. Comparison of the electrical angle, field current, rotor flux and torque when  $R_r^* = 2R_r$ .

values are:

$$\psi_r^* / \psi_r^c = 1.81 \quad (14)$$

$$T_e^* / T_e^c = 1.76 \quad (15)$$

And the results calculated by equations (9) and (13) are:

$$\psi_r^* / \psi_r^c = \sqrt{\frac{I_M^2 + I_T^2}{I_M^2 + \left(\frac{R_r}{R_r^*}\right)^2 I_T^2}} = 1.87 \quad (16)$$

$$T_e^* / T_e^c = \frac{I_M^2 + I_T^2}{\frac{R_r}{R_r^*} I_M^2 + \frac{R_r}{R_r^*} I_T^2} = 1.75 \quad (17)$$

Formula (14) is equal to (16) and formula (15) is equal to (17). Therefore, the rotor resistance error theory is quantitatively verified. When  $R_r^* > R_r$ , Fig. 4 and Fig. 5 show that the electrical angle in the first frame is ahead of the real value in the second frame and that the electrical speed is the same in the two frames, and the field current and rotor flux in the first frame are less than the real values in the second frame. This is the same in reverse. The magnetic torque is not only correlated with rotor resistance error.

### III. PARAMETER ESTIMATION ALGORITHM

#### A. Rotor Flux Estimation Theory

In the M-T axes synchronously rotating reference frame,

the dynamic model of induction machines can be expressed with the following 'voltage model':

$$\begin{cases} U_M = (R_s + \sigma L_s P) I_M + (L_m / L_r) P \psi_{rM} - \omega_{se} [\sigma L_s I_T + (L_m / L_r) \psi_{rT}] \\ U_T = (R_s + \sigma L_s P) I_T + (L_m / L_r) P \psi_{rT} + \omega_{se} [\sigma L_s I_M + (L_m / L_r) \psi_{rM}] \end{cases} \quad (18)$$

In steady state, the following is considered:

$$P I_s = 0, P \psi_r = 0 \quad (19)$$

Equation (18) becomes:

$$\begin{cases} U_M = R_s I_M - \omega_{se} [\sigma L_s I_T + (L_m / L_r) \psi_{rT}] \\ U_T = R_s I_T + \omega_{se} [\sigma L_s I_M + (L_m / L_r) \psi_{rM}] \end{cases} \quad (20)$$

For the vector control, the M-axis is aligned with the rotor flux vector. Therefore:

$$\psi_{rT} = 0, \psi_{rM} = L_m I_M \quad (21)$$

Substituting (21) into (20) yields:

$$\begin{cases} U_M = R_s I_M - \omega_{se} \sigma L_s I_T \\ U_T = R_s I_T + \omega_{se} L_s I_M \end{cases} \quad (22)$$

Equation (22) points out the relationship between the real voltage and the real current in the function of the real rotor resistance  $R$  in the steady state. There is no doubt that it can be applied to the third frame. Since the values in the second frame are all real and in the function of the real rotor resistance, it can be considered to be one special condition of  $R_r^* = R_r$ . Equation (22) can be applied to the second frame and the following is obtained:

$$\begin{cases} U_M^c = R_s I_M^c - \omega_{se}^c \sigma L_s I_T^c \\ U_T^c = R_s I_T^c + \omega_{se}^c L_s I_M^c \end{cases} \quad (23)$$

The reactive power  $Q$  of the IM can be expressed as:

$$Q = |U_s| \cdot |I_s| \cdot \sin \varphi \quad (24)$$

$\varphi$  is the angle between the stator voltage vector and the stator current vector.

The voltage vector and rotor current vector can be written as:

$$\begin{cases} \dot{U}_s = U_\alpha + j U_\beta = U_M^* + j U_T^* = U_M^c + j U_T^c \\ \dot{I}_s = I_\alpha + j I_\beta = I_M^* + j I_T^* = I_M^c + j I_T^c \end{cases} \quad (25)$$

According to the definition of the reactive power,  $Q$  can be rewritten as:

$$Q_1 = U_\beta \cdot I_\alpha - U_\alpha \cdot I_\beta \quad (26a)$$

$$Q_2 = U_T^* \cdot I_M^* - U_M^* \cdot I_T^* \quad (26b)$$

$$Q_3 = U_T^c \cdot I_M^c - U_M^c \cdot I_T^c \quad (26c)$$

$$Q = Q_1 = Q_2 = Q_3 \quad (26d)$$

Substituting (23) into 26(c) yields:

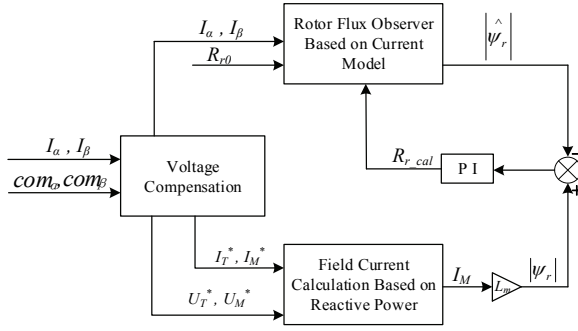


Fig. 6. Scheme of rotor resistance identification.

$$Q = \omega_{se}^c L_s (I_M^2 + \sigma I_T^2) \quad (27)$$

According to the projecting relationship in the first and second frame, the following can be obtained:

$$I_s^{c2} = I_M^2 + I_T^2 = I_s^{*2} = I_M^{*2} + I_T^{*2} \quad (28)$$

Substituting (28) and (7) into (27) yields the real rotor flux:

$$I_M^c = \sqrt{\frac{Q_2 - \sigma \omega_{se}^* L_s I_s^{*2}}{\omega_{se}^* L_s (1 - \sigma)}} \quad (29)$$

All of the variables in (29) can be acquired in one steady-state condition. The field current in the second frame can be obtained without any adaptation. Moreover, the solving process eliminates the stator resistance. The change of the stator resistance does not affect the result.  $\omega_{se}^*$  is the electrical speed used in the control system. Equation (6) is workable even when the rotor speed is not accurate. Equation (29) can be applied to conditions where there is rotor speed error.

### B. Rotor Resistance Estimation Theory

Substituting (29) into (8) yields the real rotor flux:

$$\psi_r^c = L_m \sqrt{\frac{Q_2 - \sigma \omega_{se}^* L_s I_s^{*2}}{\omega_{se}^* L_s (1 - \sigma)}} \quad (30)$$

According to (9) and (30), the real value of  $R_r$  can be determined:

$$R_r = \sqrt{\frac{Q_2 L_m^2 I_s^{*2} - \sigma \omega_{se}^* L_s I_s^{*4}}{\omega_{se}^* L_s (1 - \sigma) \psi_r^c I_T^2} - \frac{I_M^2}{I_T^2}} \times R_r^* \quad (31)$$

However, equation (31) includes high order terms that make the result unstable when the control system bears with jitters. It can just be used to estimate the probable value of  $R_r$ .

According to (1), it is possible obtain the rotor flux observer based on the current model:

$$P\hat{\psi}_r = \left(-\frac{R_r}{L_r} I + \omega_{re} J\right) \hat{\psi}_r + \frac{L_m R_r}{L_r} I_s \quad (32)$$

This section adopts the MRAS method to identify rotor resistance. Equation (30) is used as a reference model and (32) is used as an adjustable model. An adaptive mechanism uses the rotor flux error to adjust the rotor resistance. Considering

voltage compensation, Fig. 6 shows the identification scheme.

### C. Stator Resistance Estimation Theory

Since equation (27) eliminates variable stator resistance, rotor flux identification is independent of the stator resistance. It is possible to utilize a rotor flux observer based on a voltage model to estimate stator resistance. According to (1), a rotor flux observer based on the voltage mode is shown as:

$$P\hat{\psi}_r = \frac{L_r}{L_m} (U_s - R_s I_s - \sigma L_s P I_s) \quad (33)$$

Since stator current acquisition contains zero drift, the integral of the stator current can cause integral saturation and the calculated rotor flux error. A high pass filter module is taken to filter the zero drift in this section. However, the high pass filter changes the amplitude and angle of the rotor flux. Thus, a compensation should be used.

Suppose:

$$e_s = U_s - R_s I_s \quad (34)$$

Equation (33) can be rewritten as:

$$P\hat{\psi}_r = \frac{L_r}{L_m} \left(\frac{1}{s} e_s - \sigma L_s I_s\right) \quad (35)$$

Suppose:

$$\frac{1}{s} e_s - \sigma L_s I_s = \sin(\omega_{se} t + \theta_1) \quad (36)$$

Considering the zero drift of the stator current, it is possible to obtain:

$$\hat{\psi}_r = \frac{L_r}{L_m} (\sin(\omega_{se} t + \theta_1) + \int a) \quad (37)$$

In (37),  $\theta_1$  is the initial angle and 'a' is the zero drift value.

When cascading a high pass filter, (37) can be written as:

$$\hat{\psi}_r = \frac{L_r}{L_m} (\sin(\omega_{se} t + \theta_1) + \int a) \frac{s}{s + \omega_c} \quad (38)$$

In (38),  $\omega_c$  is the cut-off frequency of the high pass filter.

Suppose:

$$A = (\sin(\omega_{se} t + \theta_1) + \int a) \frac{s}{s + \omega_c} \quad (39)$$

It is possible to obtain:

$$\frac{dA}{dt} + \omega_c A = \omega_s \cos(\omega_{se} t + \theta_1) \quad (40)$$

Solving (40) yields:

$$A = C e^{-\omega_c t} + \omega_s \frac{\sin(\omega_{se} t + \theta_2)}{\sqrt{\omega_c^2 + \omega_s^2}} + \frac{a}{\omega_c} \quad (41)$$

Since the zero drift 'a' is small,  $a/\omega_c$  can be ignored. Considering  $A(0) = 0$ , it is possible to obtain the value of 'C'. The exact solution of 'A' can be expressed as:

$$A = -\omega_{se} \frac{\sin \theta_2}{\sqrt{\omega_c^2 + \omega_{se}^2}} e^{-\omega_c t} + \omega_{se} \frac{\sin(\omega_{se} t + \theta_2)}{\sqrt{\omega_c^2 + \omega_{se}^2}} \quad (42)$$

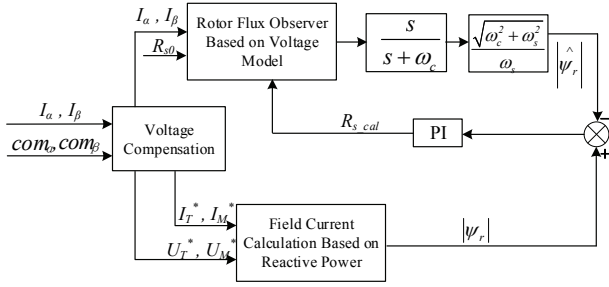


Fig. 7. Schematic of stator resistance identification.

In (42),  $\theta_2$  is the angle after conversion. With an increase in time, 'A' can be written as:

$$A = \omega_{se} \frac{\sin(\omega_{se}t + \theta_2)}{\sqrt{\omega_c^2 + \omega_{se}^2}} \quad (43)$$

Without a high pass filter, 'A' is shown as:

$$A = \sin(\omega_{se}t + \theta_1) \quad (44)$$

Through a comparison of (43) and (44), the amplitude and phase position of 'A' have changed after the high pass filter. Typically, the amplitude without a filter is  $\sqrt{\omega_c^2 + \omega_{se}^2} / \omega_{se}$  times bigger than that with a filter. Therefore, the amplitude of the rotor flux with a filter should be multiplied by  $\sqrt{\omega_c^2 + \omega_{se}^2} / \omega_{se}$  to get the real value.

Since (29) can be applied when the rotor speed is unknown and (33) does not contain a variable rotor speed or rotor resistance, the stator resistance can be obtained without a rotor speed or rotor resistance. The scheme of the stator resistance identification is shown in Fig. 7.

#### IV. IMPLEMENTATION ISSUES

In the above section, the actual stator voltages are assumed to be equal to their command values. However, in order to prevent short circuits of the phase legs, the insertion of dead time is carried out [21]. In addition, there is a time delay of the digital controller. The insertion of dead time in space vector pulse width modulation (SVPWM) and time delays can cause phase voltage distortion or the zero-current clamping phenomenon, degrading the quality of stator voltage and stator current. Thus, analysis and compensation of voltage distortions are necessary.

Since voltage distortion has been discussed many times, it will not be derived in detail here. The phase voltage error is shown as:

$$\begin{cases} \Delta U_{\alpha} = \frac{4}{\pi} \Delta U \left\{ \sin \theta + \sum_{k=1}^{\infty} \left[ \frac{\sin(6k-1)\theta}{6k-1} + \frac{\sin(6k+1)\theta}{6k+1} \right] \right\} \\ \Delta U_{\beta} = \frac{4}{\pi} \Delta U \left\{ -\cos \theta + \sum_{k=1}^{\infty} \left[ \frac{\cos(6k-1)\theta}{6k-1} - \frac{\cos(6k+1)\theta}{6k+1} \right] \right\} \end{cases} \quad (45)$$

Where:

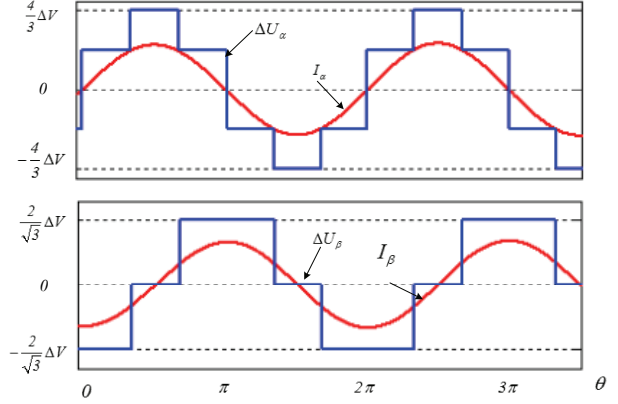


Fig. 8. Phase relation between the voltage distortion and current.

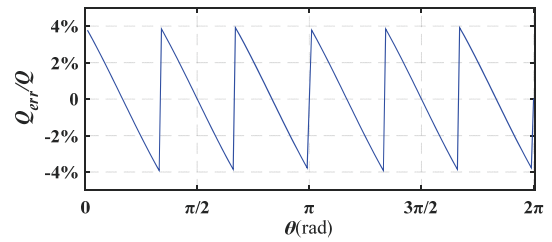


Fig. 9. Error in the reactive power.

$$\Delta U = U_{bat} \frac{T_{DT}}{T_{PWM}}$$

The symbol ' $T_{DT}$ ' is the dead time period.

From (45), it can be known that voltage distortion mainly includes the  $6k \pm 1$ th harmonics. The phase relation between the voltage distortion and current is shown in Fig. 8.

Since the  $\alpha$ -axis phase current is 90 degrees ahead of the  $\beta$ -axis phase current, it can be supposed that:

$$\begin{cases} I_{\alpha} = I_{mod} \sin \theta \\ I_{\beta} = -I_{mod} \cos \theta \end{cases} \quad (46)$$

The symbol ' $I_{mod}$ ' is the current amplitude.

By substituting (45) and (46) into (26a), the reactive power error  $Q_{err}$  can be expressed as:

$$\frac{Q_{err}}{Q} = \frac{4}{\pi} \frac{T_{DT}}{T_{PWM}} \frac{1}{\sin \varphi} \sum_{k=1}^{\infty} \frac{12k \sin 6k\theta}{(6k-1)(6k+1)} \quad (47)$$

Suppose  $T_{DT} = 3 \mu s$ ,  $T_{PWM} = 100 \mu s$  and  $\sin \varphi = 0.5$ , it is possible to obtain the reactive power error in Fig. 9.

The angle  $\varphi$  between the voltage and current is correlated with the relationship between the reactive power and the active power. When increasing the load torque, the active power increases and  $\varphi$  decreases, which can cause a larger reactive power error. Phase voltage compensation is carried out to enhance the accuracy and robustness.

In the simulation and experiment, the phase voltage error is obtained by phase voltage reconstruction [21], which requires the precise duty cycle of every phase. Take phase  $U$  as an example:



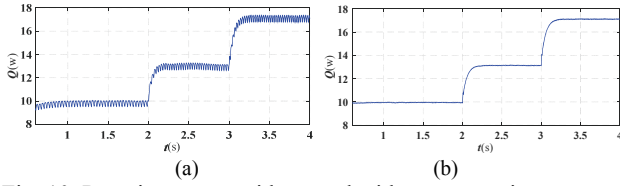
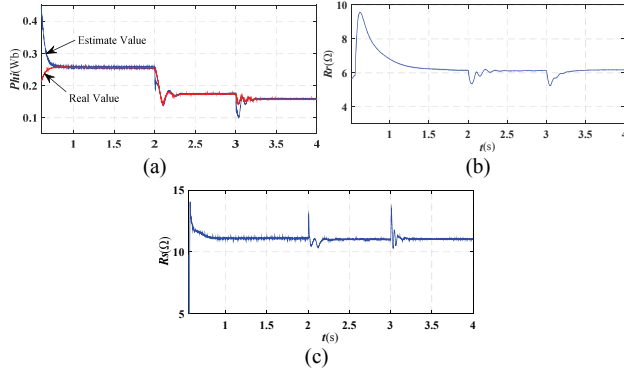


Fig. 10. Reactive power without and with compensation.

Fig. 11. Identification results when  $R_r^* = 10\Omega$  and  $\omega_r = 100rpm$ .

$$Duty\_U = \frac{\int V_{u0}}{V_{DC} \cdot T_{PWM}} \quad (48)$$

Where  $Duty\_U$  is the real duty cycle and  $T_{PWM}$  and  $V_{u0}$  are the PWM period and terminal voltage of phase  $U$ , respectively. The phase voltage reconstruction and phase voltage error can be obtained after acquisition of the duty cycle.

Considering the phase voltage compensation, the schemes of the rotor and stator resistance are shown in Fig. 6 and Fig. 7.

## V. SIMULATION AND EXPERIMENTAL RESULTS

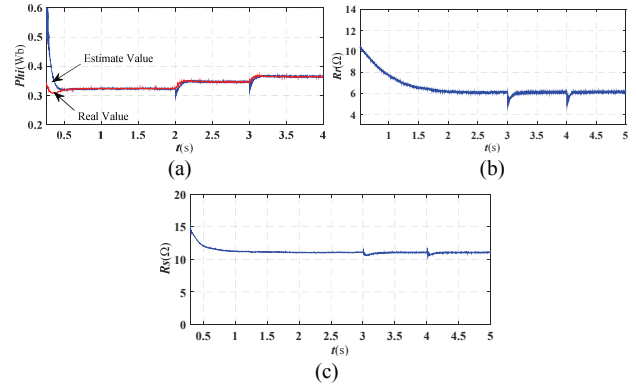
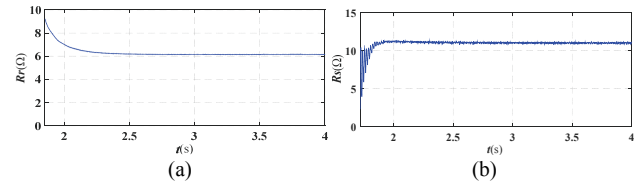
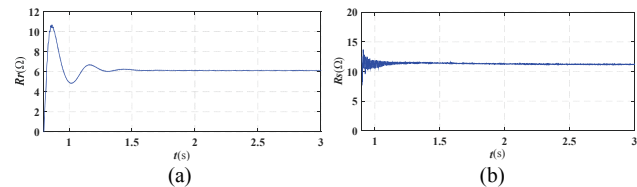
### A. Simulation Results

An induction motor drive with IFOC is established in Simulink to verify the theory proposed in this paper. The parameters of the motor are shown in Table II in section II. Since the rotor resistance varies slowly with time, it is presumed to be constant. The period of the PWM is set at  $100\mu s$ .

Fig. 10 shows the reactive power  $Q$  with and without voltage compensation. The rotor resistance is set to the true value. For a better demonstration of their effects, the load torque is set to 40%, 70% and 100% of the rated load. When compared with Fig. 10(b), Fig. 10(a) fluctuates roughly. When the load torque increases,  $Q$  bears with an intensive fluctuation.

In the following simulations, the induction motor operates with voltage compensation. The rotor resistance is initially set to a wrong value. The observer is activated when the motor starts up to the commanded speed and load torque.

In order to verify the identification response when the load torque changes, the load torque is set to 40%, 70% and 100%

Fig. 12. Identification results when  $R_r^* = 4\Omega$  and  $\omega_r = 100rpm$ .Fig. 13. Identification results when  $R_r^* = 10\Omega$ ,  $\omega_r = 1000rpm$  and the rated load torque = 50%.Fig. 14. Identification results when  $R_r^* = 4\Omega$ ,  $\omega_r = 1000rpm$  and the rated load torque = 50%.

of the rated load in Fig. 11 and Fig. 12. Fig. 11(a) and Fig. 12(a) show that the rotor flux observer can keep tracking the rotor flux feedback from the induction motor model. Since the proposed method can only be applied to the steady-state condition, the identification results fluctuate when the control system is unstable. Fig. 11 and Fig. 12 show that the identification results can converge to the real value after the load torque changes. The theory is verified by the simulation in this section.

### B. Experimental Results

The experiment takes a TMS320F28335 as the digital signal processor (DSP). The feedback circuit in [21] is applied in the experiment. The motor and IGBT parameters are shown in Table II and Table III, respectively.

The experimental setup is shown in Fig. 15. Two induction motors are used to act as a load motor and a drive motor. A torque sensor is used to obtain accurate torque in real time. Unless mentioned, the test conditions in the following experiments are the same as those in the simulations.

Fig. 16 shows reactive power  $Q$  without and with voltage compensation. When compared with Fig. 16(b), Fig. 16(a) fluctuates roughly. In Fig. 17 and Fig 18, the load torque is

TABLE III  
PARAMETERS OF AN IGBT (POWEREX PS21765)

Variables	QUANTITY	Unit
Amperes/Volts	20/600	A/V
Collector-Emitter Saturation Voltage	0.8	V
Diode Forward Voltage	0.7	V

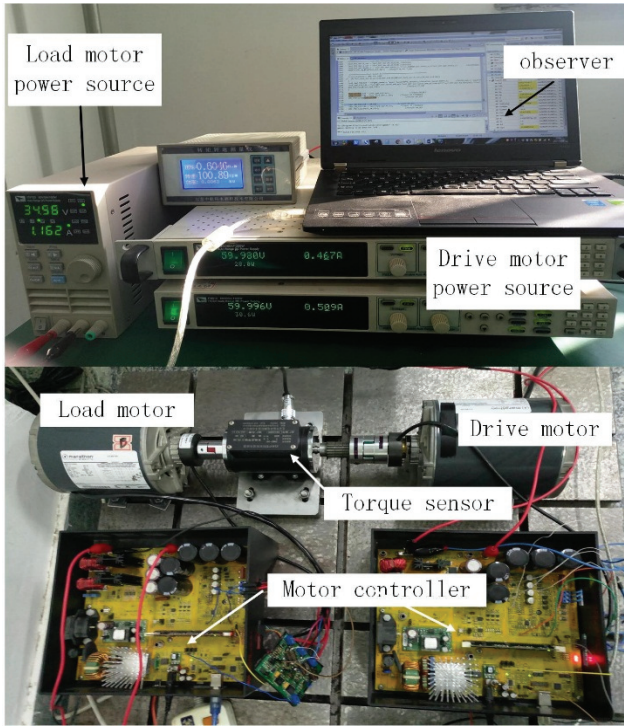


Fig. 15. Experimental setup.

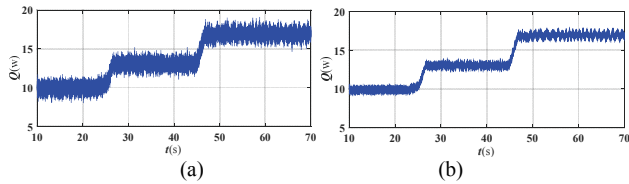


Fig. 16. Reactive power without and with compensation.

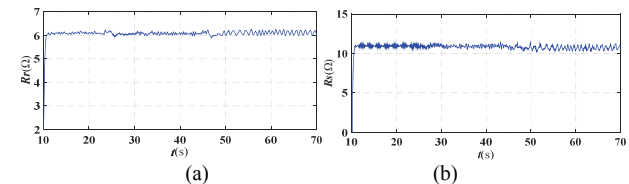


Fig. 17. Identification results when  $R_r^* = 10\Omega$  and  $\omega_r = 100rpm$ .

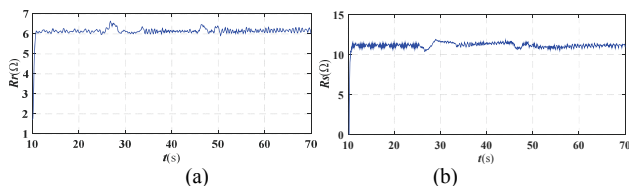


Fig. 18. Identification results when  $R_r^* = 4\Omega$  and  $\omega_r = 100rpm$ .

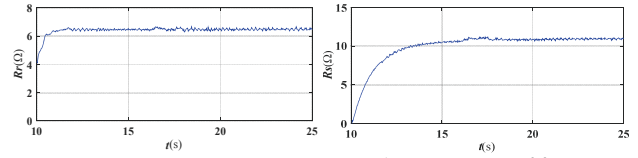


Fig. 19. Identification results when  $R_r^* = 4\Omega$ ,  $\omega_r = 500rpm$  and the rated load torque = 50%.

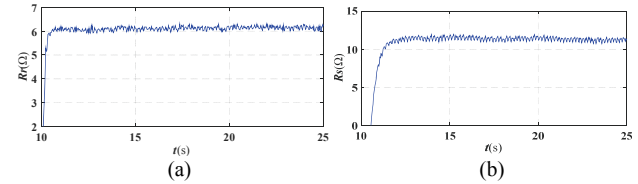


Fig. 20. Identification results when  $R_r^* = 10\Omega$ ,  $\omega_r = 1000rpm$  and the rated load torque = 50%.

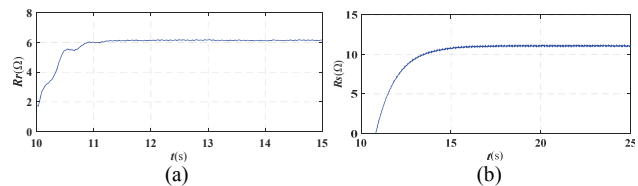


Fig. 21. Identification results when  $R_r^* = 4\Omega$ ,  $\omega_r = 1000rpm$  and the rated load torque = 50%.

set to 40%, 70% and 100% of the rated load at 10s, 25s and 45s, respectively. In Fig. 17-Fig. 21 the adaptation scheme is tested at three speeds, two rotor resistances and three different load conditions. The rotor resistance and stator resistance are adjusted to real value under the above conditions.

## VI. CONCLUSION

In this paper, a novel parameter identification method was proposed. Salient features of the system are its simplicity and directness, since the real rotor flux can be calculated without any adaptation. The influence of the rotor resistance error is analyzed in three coordinate frames and real rotor flux is derived from the relationships among the second frame and other frames in the steady-state condition of an induction motor. Based on estimated rotor flux, the rotor resistance and stator resistance are identified using MRAS. Moreover, the rotor flux and stator resistance identification methods are independent of the rotor resistance. Voltage distortion which can severely affect reactive power calculations are compensated. Simulations and experiments were carried out under several typical conditions. The obtained results verify the identification scheme.

## ACKNOWLEDGMENT

The authors gratefully acknowledge the financial support of the Fundamental Research Funds for the Central Universities (HIT.NSRIF.201705) and Natural Science Foundation of Shandong Province (ZR2017MEE011).



## REFERENCES

- [1] R. Krishnan and A. S. Bharadwaj, "A review of parameter sensitivity and adaptation in indirect vector controlled induction motor drive systems," *IET Power Electron*, Vol. 6, No. 4, pp. 695-703, Oct. 1991.
- [2] K. B. Nordin and D. W. Novotny, "The influence of motor parameter deviations in feedforward field orientation drive systems," *IEEE Trans. Ind. Appl*, Vol. 21, No. 4, pp. 1009-1015, Jul./Aug. 1985.
- [3] R. Krishnan and F. C. Doran, "Study of parameter sensitivity in high-performance inverter-fed induction motor drive systems," *IEEE Trans. Ind. Appl*, Vol.23, No.4, pp. 623-635, Jul./Aug. 1987.
- [4] D. Chatterjee, "Impact of core losses on parameter identification of three-phase induction machines," *IET Power Electron.*, Vol. 7, No. 12, pp. 3126-3136, Dec. 2014.
- [5] M. Dal, R. Teodorescu and F. Blaabjerg, "Complex state variable- and disturbance observer-based current controllers for AC drives: an experimental comparison," *IET Power Electron*, Vol. 6, No. 9, pp. 1792-1802, Nov. 2013.
- [6] K. Wang, B. Chen, G. T. Shen, W. X. Yao, K. Lee, and Z. Y. Lu, "Online updating of rotor time constant based on combined voltage and current mode flux observer for speed-sensorless AC drives," *IEEE Trans. Ind. Electron*, Vol. 61, No. 9, pp. 4583-4593, Sep. 2014.
- [7] M. W. Deger, J. M. Guerrero, and F. Briz, "Slip-gain estimation in field-orientation-controlled induction machines using the system transient response," *IEEE Trans. Ind. Appl*, Vol. 42, No. 3, pp. 702-711, May/June. 2006.
- [8] S. Wang, V. Dinavahi, and J. Xiao, "Multi-rate real-time model-based parameter estimation and state identification for induction motors," *IET Electr. Power Appl.*, Vol. 7, No. 1, pp. 77-86, Jan. 2013.
- [9] C. Korlinchak and M. Comanescu, "Sensorless field orientation of an induction motor drive using a time-varying observer," *IET Electr. Power Appl*, Vol. 55, No.3, pp. 353-361, Jul. 2012.
- [10] J. A. Riveros, A. G. Yepes, and F. Barrero, "Parameter identification of multiphase induction machines with distributed windings - Part 2: Time-domain techniques," *IEEE Trans. Energy Convers.*, Vol. 27, No. 4, pp. 1067-1077, Dec. 2012.
- [11] V. R. Jevremovic, V. Vasic, D. P. Marcetic, and B. Jefrenic, "Speed-sensorless control of induction motor based on reactive power with rotor time constant identification," *IET Electr. Power Appl.*, Vol. 4, No. 6, pp. 462-473, Jul. 2010.
- [12] K. Tungpimolrut, F.-Z. Peng, and T. Fukao, "Robust vector control of induction motor without using stator and rotor circuit time constants," *IEEE Trans. Ind. Appl.*, Vol. 30, No. 5, pp. 1241-1246, Sep./Oct. 1994.
- [13] S. Maiti, C. Chakraborty, and Y. Hori, "Model reference adaptive controller-based rotor resistance and speed estimation techniques for vector controlled induction motor drive utilizing reactive power," *IEEE Trans. Ind. Electron.*, Vol. 5, No. 2, pp. 594-600, Feb. 2008.
- [14] X. Yu, M. W. Dunnigan, and B. W. Williams, "A novel rotor resistance identification method for an indirect rotor flux-orientated controlled induction machine system," *IET Power Electron.*, Vol. 17, No. 3, pp. 353-364, May 2002.
- [15] F. L. Mapelli, A. Bezzolato, and D. Tarsitano, "A rotor resistance MRAS estimator for induction motor traction drive for electrical vehicles," in *Proc. ICEM, Marseille*, pp. 823-829, Sep. 2012.
- [16] L. Garces, "Parameter adaption for the speed-controlled static AC drive with a squirrel-cage induction motor," *IEEE Trans. Ind. Appl.*, Vol. IA-16, No. 2, pp.173-178, Mar./Apr. 1980.
- [17] P. Cao, X. Zhang, and S. Yang, "A unified model based analysis of MRAS for online rotor time constant estimation in induction motor drive," *IEEE Trans. Ind. Electron*, Vol. 64, No. 6, pp. 4361-4371, Jun. 2017.
- [18] J. Kan, K. Zhang, and Z. Wang, "Indirect vector control with simplified rotor resistance adaptation for induction machines," *IET Power Electron.*, Vol. 8, No. 7, pp. 1284-1294, Jul. 2015.
- [19] H. Bin, Q. Wen, and L. Hai, "A novel on-line rotor resistance estimation method for vector controlled induction motor drive," in *Proc. Conf. Rec. IEEE IPEMC Conf*, Vol. 2, pp. 137-147, Aug. 1992.
- [20] M. S. N. Said and M. E. H. Benbouzid, "Induction motors direct field oriented control with robust on-line tuning of rotor resistance," *IEEE Trans. Energy Convers.*, Vol. 14, No. 4, pp. 1038-1042, Dec. 1999.
- [21] D. Wang, B. Yang, C. Zhu, C. Zhou, and J. Qi, "A feedback-type phase voltage compensation strategy based on phase current reconstruction for ACIM drives," *IEEE Trans. Power Electron.*, Vol. 29, No. 9, pp. 5031-5043, Sep. 2014.



**Mingyu Wang** received his B.S. and M.S. degrees in Automotive Engineering from the Harbin Institute of Technology, Weihai, China, in 2014 and 2016, respectively. He is presently working towards his Ph.D. degree in Mechano-Electronic Engineering for Electric Vehicles at the Harbin Institute of Technology. His current research interests

include e-PMSM emulations and electric vehicle motor traction systems.



**Dafang Wang** was born in Liaoning, China, in 1978. He received his M.S. degree in Automotive Engineering from the Harbin Institute of Technology, Harbin, China, in 2002; and his Ph.D. degree in Automotive Engineering from the Beijing Institute of Technology, Beijing, China, in 2008. He is presently working as a Professor at the

Harbin Institute of Technology, Weihai, China. His current research interests include new energy and intelligent connected vehicles.



**Guanglin Dong** was born in Shandong, China, in 1995. He received his B.S. degree in Vehicle Engineering from the Harbin Institute of Technology, Weihai, China, in 2017, where he is presently working towards his M.S. degree in Vehicle Engineering. His current research interests include the hardware-in-the-loop (HIL) systems of electric vehicles

and motor traction systems.



**Hui Wei** was born in Fujian, China, in 1994. He received his B.S. degree in Vehicle Engineering from the Harbin Institute of Technology, Weihai, China, in 2017, where he is presently working towards his M.S. degree in Vehicle Engineering. His current research interests include electric vehicle motor traction systems, power loss analysis of converters and temperature analysis of IGBT power modules.



**Zexu Xu** was born in Jilin, China, in 1996. He received his B.S. degree in Vehicle Engineering from the Harbin Institute of Technology, Weihai, China, in 2018, where he is presently working towards his M.S. degree in Vehicle Engineering. His current research interests include the control and thermal analysis of the permanent magnet synchronous machines used in new energy vehicles.



**Xiu Liang** was born in Shandong, China, in 1995. She received her B.S. degree in Vehicle Engineering from the Harbin Institute of Technology, Weihai, China, in 2017, where she is presently working towards her M.S. degree in Vehicle Engineering. Her current research interests include electric vehicle motor traction systems, rapid control prototypes and hardware-in-the-loop (HIL) systems.